# The $^3$He($\vec{d}$,$p$)$^4$He reaction at low energies

W. H. Geist, C. R. Brune, H. J. Karwowski, E. J. Ludwig, and K. D. Veal
*Department of Physics and Astronomy, University of North Carolina at Chapel Hill, Chapel Hill, North Carolina 27599-3255 and Triangle Universities Nuclear Laboratory, Durham, North Carolina 27708-0308*

G. M. Hale
*Los Alamos National Laboratory, Los Alamos, New Mexico 87545*

(Received 2 April 1999; published 19 October 1999; publisher error corrected 14 May 2003)

Angular distributions of cross sections and complete sets of analyzing powers for the $^3$He($\vec{d}$,$p$)$^4$He reaction have been measured at five energies between $E_d=60$ and 641 keV. The energy dependence of the cross section was also measured from 245 to 685 keV, and the absolute cross section was determined at $E_d=426$ keV. The data have been included in an $R$-matrix analysis of the $^5$Li system. The bare-nuclear cross section derived from the $R$-matrix parametrization was used to determine the electron screening potential. [S0556-2813(99)00911-5]

PACS number(s): 25.10.+s, 24.70.+s, 26.35.+c, 27.10.+h

## I. INTRODUCTION

The $^3$He($d$,$p$)$^4$He reaction ($Q=18.35$ MeV) has been studied for several decades for both fundamental and practical purposes. This reaction is dominated at low energies by a broad $J^\pi=\frac{3}{2}^+$ $S$-wave resonance in $^5$Li located at a deuteron energy near 420 keV. If the reaction proceeds entirely via this partial wave, the observables can be easily calculated [1]. It was found, however [2,3], that other reaction channels with different $J^\pi$ and/or orbital angular momenta are also present at these low energies and must be accounted for to accurately describe the observables. A recent and detailed account of how the polarization observables depend on the underlying partial wave amplitudes is given in Ref. [4].

There are a number of motivations for continued study of $^3$He($d$,$p$)$^4$He reaction. The data obtained for this reaction can be used in a global $R$-matrix analysis of the $^5$Li system. This type of analysis is useful for determining the properties of the many broad levels in $^5$Li. In addition, the analysis can be used to predict unmeasured observables, including the $S$ factor near zero energy which is important for electron screening determinations.

The $^3$He($d$,$p$)$^4$He reaction plays a very important role in primordial nucleosynthesis of the light elements D, $^3$He, $^4$He, and $^7$Li [5]. Recent measurements of the D/H ratio in high-redshift gas clouds have determined the primordial D abundance within 10% [6]. These measurements place tight constraints on big-bang nucleosynthesis, but some conclusions are limited by the precision of the nuclear physics input data. For the parameter space normally considered, big-bang nucleosynthesis is sensitive to the $^3$He($d$,$p$)$^4$He cross section in the range $100\lesssim E_d\lesssim 500$ keV. There are several previous measurements of the absolute cross section for $^3$He($d$,$p$)$^4$He in this energy range [7–14], but they disagree by up to 30%. Precise measurements of the cross section are also useful for nuclear microanalysis aiming to determine the concentration of deuterium or $^3$He in a substrate [13].

The $^3$He($d$,$p$)$^4$He reaction is an important case for experimentally studying the electron screening effect [15]. This effect manifests itself when the electrons of the target atoms screen the positively charged projectile from the full Coulomb potential of the target nucleus. As a result the projectile sees a reduced Coulomb barrier, leading to an enhancement of the measured cross section $\sigma_{\rm exp}$ over the bare nuclear cross section $\sigma_{\rm BN}$. It is important to understand this effect, as certain reactions of astrophysical interest require $\sigma_{\rm BN}$ to be known at very low energies. Since the $^3$He($d$,$p$)$^4$He reaction shows a very large screening enhancement at experimentally accessible energies, the study of this reaction allows for a better understanding of this effect.

The $^3$He($d$,$p$)$^4$He reaction also has excellent characteristics for use in the determination of the tensor polarization of deuteron beams [16]. The advantages of this reaction as a polarization monitor are its high $Q$ value and large tensor analyzing powers which vary smoothly with energy. The assumption of a pure $\frac{3}{2}^+$ $S$-wave resonance yields [1]

$$A_y(\theta)=0, \tag{1}$$

$$A_{yy}(\theta)=\tfrac{1}{2}, \tag{2}$$

$$A_{xz}(\theta)=-\tfrac{3}{2}\cos\theta\,\sin\theta, \tag{3}$$

$$A_{zz}(\theta)=\tfrac{1}{2}(1-3\cos^2\theta), \tag{4}$$

and isotropic $\sigma(\theta)$. The high-precision measurements of the tensor analyzing powers (TAPs) presented here determine deviations from these formulas and enable a more accurate calibration of polarization measurements.

Below $E_d=1$ MeV only two experiments have measured angular distributions of analyzing powers. Complete sets of analyzing powers were measured by Leemann *et al.* [2] at $E_d=430$ keV, and by Garrett and Lindstrom [3] at $E_d=344$, 465, and 727 keV. In addition, Dries *et al.* [17] measured $A_{zz}(0^\circ)$ for $E_d=480$ and 760 keV. In these experiments the data were found to deviate from the relationships given by Eqs. (1)–(4) indicating that transitions involving higher partial waves are present in the entrance channel.

In the present work we report measurements of angular distributions of both cross sections and deuteron vector analyzing power (VAP) $A_y$ and TAPs $A_{yy}$, $A_{zz}$, and $A_{xz}$ at mean deuteron laboratory reaction energies of $E_d=60$, 99, 199, 424, and 641 keV. Also, the relative energy dependence

 

of the cross section was measured at energies from 245 to 685 keV and the absolute total cross section was determined at $E_d = 426$ keV. Some of these measurements utilized the inverse kinematics $^2$H($^3$He,$p$)$^4$He reaction as discussed below. These results are reported throughout the paper in the $^3$He($d$,$p$)$^4$He reaction frame for consistency.

## II. EXPERIMENTAL PROCEDURE

Measurements of the cross sections and complete sets of analyzing powers for the $^3$He($d$,$p$)$^4$He reaction were undertaken using the low-energy beam facility (LEBF) at the Triangle Universities Nuclear Laboratory. This facility consists of an atomic-beam polarized ion source [18], the minitandem accelerator [19], and the high-voltage scattering chamber [20]. It allows measurements of reactions induced by polarized deuterons in the 40 to 680 keV energy range as described below.

### A. Beams

The atomic-beam polarized ion source is capable of producing positively or negatively charged beams of polarized or unpolarized deuterons and negatively charged beams of $^3$He at energies up to 80 keV. For beam energies greater than 80 keV the minitandem accelerator and/or high-voltage scattering chamber were used to further increase the beam energy. The minitandem operates in open air and accelerates a negatively charged beam towards a positive potential of up to 200 kV placed on the terminal. The beam undergoes charge exchange with a $\sim 2$-$\mu$g/cm$^2$ carbon foil in the terminal and is then further accelerated leaving the minitandem. The LEBF bending magnet, located after the minitandem, is used to analyze the charge state and steer the beam into the high-voltage chamber where the measurements were performed. For deuteron beam energies greater than 480 keV, the highest energy attainable by biasing only the minitandem, the high-voltage scattering chamber is also biased by up to $-200$ kV. When the beam energy required is less than 280 keV, the more intense positive beam from the polarized ion source was used. In this case the minitandem accelerator was grounded and the carbon foil was removed allowing the beam to drift through and the high-voltage scattering chamber was biased to accelerate the beam to the required energy. The beam energy was calibrated to $\pm 1$ keV using the 240.0- and 340.5-keV resonances in $^{19}$F($p,\alpha\gamma$) and the 405.4- and 445.8-keV resonances in $^{27}$Al($p,\gamma$). The resonance energies were taken from Ref. [21].

For the measurements that utilized a $^3$He beam, a $^3$He$^-$ beam was accelerated into the minitandem. Using the LEBF bending magnet, the $^3$He$^{++}$ charge state was analyzed and sent into the high-voltage chamber. In this operating configuration, the maximum $^3$He beam energy attainable is 1080 keV.

Three different beam polarization states were produced with the atomic beam polarized ion source: a maximum positive, a maximum negative, and an unpolarized state. The TAP data were obtained with $p_{ZZ} \approx \pm 0.80$ and $p_Z \approx \mp 0.25$, while $p_Z \approx \pm 0.50$ and $|p_{ZZ}| \leq 0.05$ were used for the VAP measurements. The spin states were cycled approximately once every second, in order to minimize the effects of slow changes in beam position, target thickness, or amplifier gain. A Wien filter allowed complete control of the beam polarization axis at the target. The spin axis was longitudinal for the $A_{zz}$ measurements, normal to the reaction plane for $A_y$ and $A_{yy}$, and 45° offset from longitudinal in the reaction plane for $A_{xz}$. The deuteron beam polarization was determined with well-calibrated polarimeters mounted in the rear of the high-voltage scattering chamber. The deuteron tensor polarimeter [16] utilizes the $^3$He($d$,$p$)$^4$He reaction while the vector polarimeter [22] uses both the $^2$H($d$,$p$)$^3$H and $^{12}$C($d$,$p$)$^{13}$C reactions. The systematic error in the polarization measurements from the calibration process is estimated to be 4.3% for the tensor polarimeter and 3.7% for the vector polarimeter.

### B. Targets and detectors

The $^3$He targets were made by implanting 17-keV $^3$He ions into 0.05-mm-thick Ta substrates [23]. Target thicknesses on the order of $10^{17}$ $^3$He/cm$^2$ were obtained. Calculations using the Monte Carlo simulation code TRIM (transport and ranges of ions in matter [24]) determined both the $^3$He implantation depth and the energy loss for deuterons traveling through the substrate to this depth. These energy losses were found to range from 4 to 9 keV for the beam energies of the present measurements. Deuterated carbon targets [25] were used with the $^2$H($^3$He,$d$)$^4$He measurements. These targets were made with plasma-assisted chemical vapor deposition of deuterated methane gas on a $\sim 0.015$-mm-thick Al foil. Target thicknesses of $(1-5)\times 10^{17}$ D/cm$^2$ were obtained. The energy loss of a 650-keV $^3$He beam in these targets was measured to be $\approx 10$ keV. The targets were positioned in the center of the scattering chamber and were mounted on an insulated target rod to allow for beam-current integration. In all the measurements the target rod was biased for electron suppression.

The reaction products were measured with 1000-$\mu$m-thick Si surface barrier detectors mounted in the 107-cm-diameter scattering chamber on tracks attached to the top and bottom plates which can be rotated independently. For the analyzing power and cross section angular distributions, three pairs of detectors separated by 20° were placed symmetrically about the beam direction to detect the outgoing protons. Tantalum foils of 0.127-mm thickness were placed in front of the detectors to slow the protons so that they would be stopped in the detectors and to prevent elastically scattered particles from entering the detectors. Detector solid angles for the 199-, 424-, and 641-keV measurements were 5.0 msr, with an angular acceptance of $\pm 1.5°$. A sample spectrum is shown in Fig. 1. For the 60- and 99-keV measurements, a larger solid angle of 25.0 msr, with an angular acceptance of $\pm 5.0°$, was used. For the cross section angular distributions, a pair of fixed-angle monitor detectors was placed out of the reaction plane. The cross section excitation function and absolute cross section measurements were performed with two pairs of detectors placed at 20° and 160° in order to detect the reaction products from the $^2$H($^3$He,$p$)$^4$He

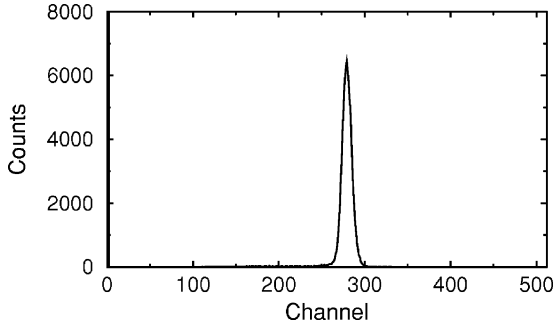


FIG. 1. Typical proton spectrum from the $^3$He($d,p$)$^4$He reaction at $E_d$=424 keV.

reaction and an additional pair of detectors placed at 140° to detect elastically scattered particles. The detectors at 160° registered only protons while the detectors at 20° collected both protons and $\alpha$ particles as shown in Fig. 2. The broad proton peak results because the protons do not stop in the detector. The 140° detector spectra, shown in Fig. 3, were used to measure the beam energy loss in the target for both plain Al backing and a deuterated carbon target on an Al backing. The beam energy loss in the deuterated carbon layer is related via Eq. (46) of Sargood [26] to the energy shift of the end point for elastically scattered deuterons.

### C. Measurements

Measurements of complete angular distributions of $\sigma$, $A_y$, $A_{yy}$, $A_{zz}$, and $A_{xz}$ were taken at five incident deuteron energies corresponding to mean reaction energies of 60, 99, 199, 424, and 641 keV. An excitation function of the total cross section was measured for deuteron energies from 245 to 685 keV. We also present a determination of the absolute cross section at 426 keV.

The analyzing power angular distributions were measured at laboratory angles from 0° to 170° in 10° steps. At the lowest two energies, and for the vector analyzing power data, 20° steps were taken.

The relative energy dependence of the cross section was obtained by accelerating a $^3$He beam through the minitandem and/or the high-voltage chamber onto a deuterated carbon target. The beam was tuned at one fixed minitandem voltage and the beam energy was adjusted over a range of 400 keV by adjusting the bias on the high-voltage chamber.

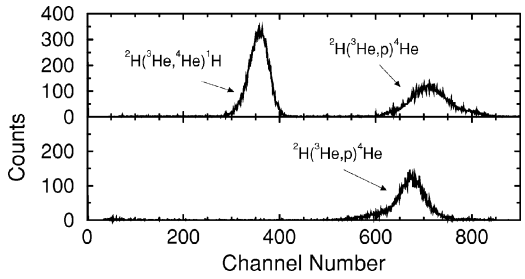


FIG. 2. Typical charged-particle spectra from the $^2$H($^3$He,$p$)$^4$He reaction. The top spectrum shows the forward-angle detector located at $\theta_{lab}$=20° and the bottom spectrum shows the back-angle detector located at $\theta_{lab}$=160°.

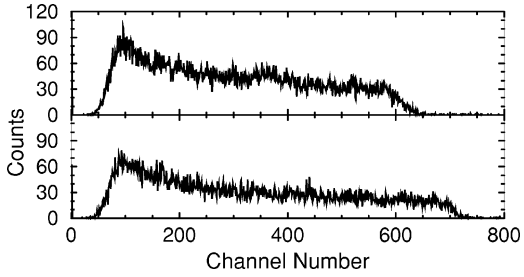


FIG. 3. Spectra of backscattered helions observed at $\theta_{lab}$ = 140°. The top figure is for elastic scattering from Al with a deuterated carbon layer and the bottom spectrum is for a plain Al target.

This procedure was then repeated at several different minitandem voltages. The beam energy was periodically retuned to a previously measured energy throughout the measurements to monitor for possible target thickness losses.

For the absolute cross section measurement, first a deuteron beam was tuned onto the target to measure the product of the target thickness times solid angle $t\Delta\Omega$. This quantity was determined using the $^2$H($d,p$)$^3$H reaction at 116 keV where the cross section is well known [27]. Next a $^3$He beam was accelerated to 651 keV, near the peak of the resonance, and the cross section was measured using the known $t\Delta\Omega$.

## III. RESULTS

### A. Cross section measurements

The measurement of the relative angular distributions consisted of taking a ratio of the counts in the movable detectors to the counts in the fixed-angle monitor detectors. The results are shown in Fig. 4. The cross section is found to be nearly isotropic at the lowest energies and becomes forward peaked at the higher energies. These trends agree with previous measurements [7,8,10,14].

The energy dependence of the relative differential cross section was obtained by taking the ratio of the counts in the detectors to the collected charge. To correct for the target thickness loss, the ratio was remeasured several times throughout the experiment at the same beam energy. The relative total cross sections were determined using our measured information about the shape of the angular distribution, since the cross section is not precisely isotropic. The excitation function was then scaled to the absolute cross section measurement as described below and is shown in Fig. 5. Within the respective errors the excitation function agrees in shape with a previous measurement [12].

The absolute total cross section at $E_d$=426 keV was determined from the absolute differential cross section measurements using the relative angular distribution measured at $E_d$=424 keV (the error from the slight difference in energy is negligible). Since the statistical error is very small ($<$0.2%) the uncertainty in the total cross section is due exclusively to systematic errors. This error is estimated to be 4.3% by adding the following errors in quadrature. There is a 1.3% scale error in the $^2$H($d,p$)$^3$H cross section data as quoted in Ref. [27]. A 3.0% error arises in the calculation of the $^2$H($d,p$)$^3$H cross section due to uncertainties in interpo-

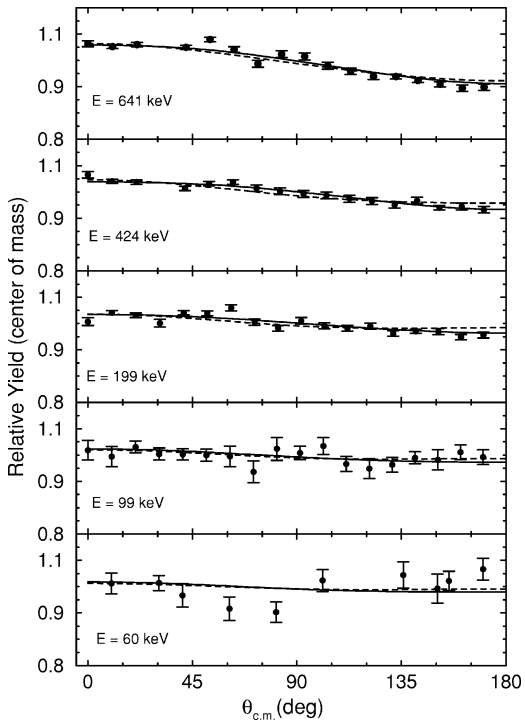


FIG. 4. Angular distributions of the relative yield for the $^3$He$(d,p)^4$He reaction. The solid line shows the *R*-matrix fit to data set A and the dashed line is for the *R*-matrix fit to data set B.

lating in energy and angle from the least-squares fit to the data. Uncertainties in the incident energy and the energy loss leads to a 2% error. A 2% error is estimated in the beam integration due to effects such as the beam hitting different spots on the target and/or leakage current from the battery used for electron suppression. The total cross section was thus determined to be $777\pm33$ mb at a deuteron energy of 426 keV. A comparison of the present result with previously measured values is shown in Table I.

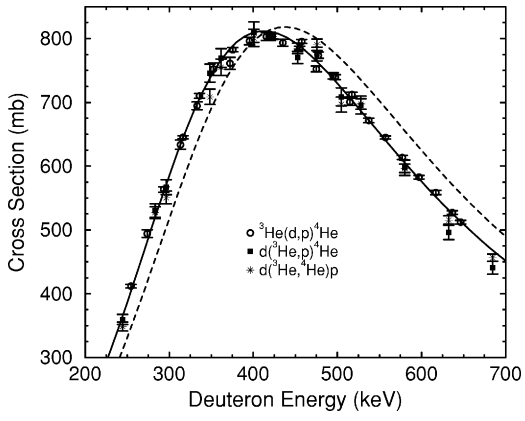


FIG. 5. Total cross sections measured for the $^3$He$(d,p)^4$He reaction. The error bars are purely statistical. The solid line shows an *R*-matrix fit to data set A and the dashed line is for the *R*-matrix fit to data set B. For comparison to the *R*-matrix fits the data were scaled by 1.03.

TABLE I. The value of the total peak cross section for the $^3$He$(d,p)^4$He reaction.

| $\sigma_{tot}$(mb) | Author |
|---|---|
| 690 | Bonner *et al.* [7] |
| $900\pm90$ | Yarnell *et al.* [8] |
| $940\pm75$ | Freier and Holmgren [9] |
| $695\pm35$ | Kunz [10] |
| $847\pm53$ | Zichang *et al.* [11] |
| $828\pm41$ | Möller and Besenbacher [12] |
| $819\pm26$ | Davies and Norton [13] |
| $777\pm33$ | Present work |

### B. Analyzing power measurements

For the determination of analyzing powers, ratios of counts in each polarized state to counts in the unpolarized state were taken and corrected for both the collected charge and dead time differences between the different spin states. The analyzing powers are then calculated from these ratios using

$$A_y=\frac{L-R}{3p_z}, \tag{5}$$

$$A_{yy}=\frac{L+R-2}{p_{zz}}, \tag{6}$$

$$A_{zz}=\frac{2(L-1)}{p_{zz}}=\frac{2(R-1)}{p_{zz}}, \tag{7}$$

$$A_{xz}=\frac{L-R}{p_{zz}}, \tag{8}$$

where $R$ and $L$ are the ratio of counts in the polarized state to unpolarized state for the right and left detectors, respectively, and the beam polarizations $p_z$ and $p_{zz}$ are determined from the polarimeter. The final plotted values are the average of both spin states.

Angular distributions of the analyzing powers are shown in Figs. 6–9. In order to more easily see the deviations from Eqs. (3) and (4), we subtracted from the data points the values expected from a pure $\frac{3}{2}^+$ *S*-wave resonance. If the reaction proceeded purely via this partial wave, the angular distributions for $A_{xz}$ and $A_{zz}$ plotted in this way would be equal to zero. The error bars include only statistical errors and not the systematic error in the polarization measurement as discussed in Sec. II A. Systematic errors due to spin-axis misalignment and finite-solid angle corrections were estimated to be negligible.

Since the current measurements were performed at different energies than the previous experiments [2,3,17,28] a straightforward comparison is not possible. It is found that the energy dependence of the present data is consistent with the previous results with the exception of the $A_{zz}$ data of Ref. [3] at $E_d=465$ and 727 keV. At these energies the data of Ref. [3] at backward angles appear to drop off much faster

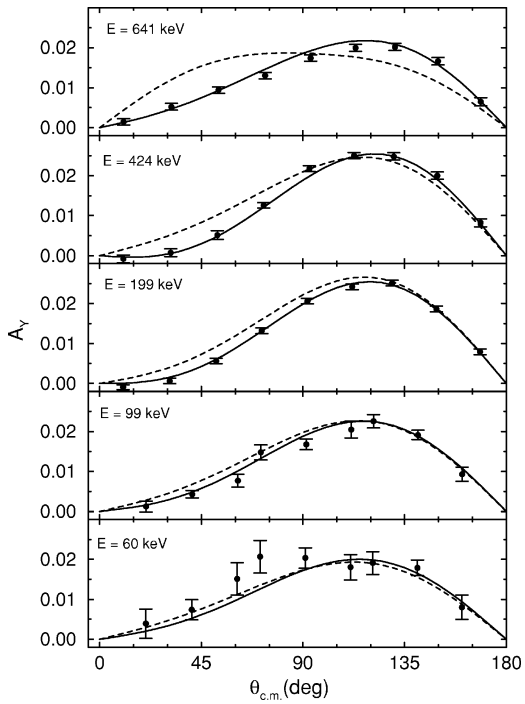


FIG. 6. Angular distributions of $A_y$ for the $^3$He$(d,p)^4$He reaction. The solid line shows an *R*-matrix fit to data set A and the dashed line is for the *R*-matrix fit to data set B. For comparison to the *R*-matrix fits the data were scaled by 1.02.

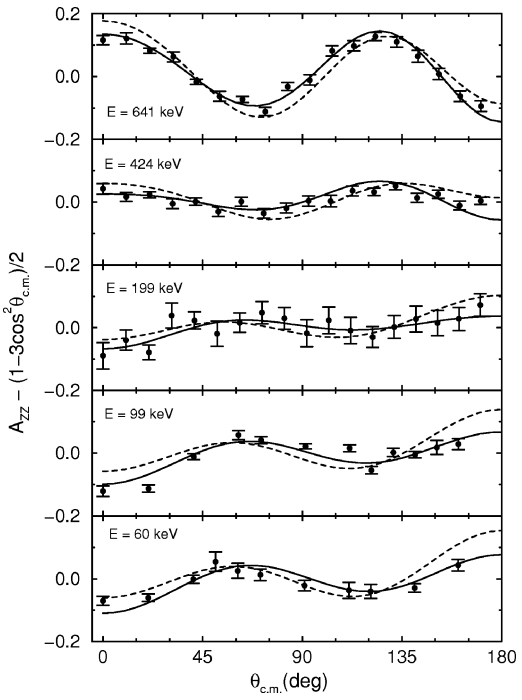


FIG. 8. Angular distributions of $A_{zz}$ (modified as described in the text) for the $^3$He$(d,p)^4$He reaction. The solid line shows an *R*-matrix fit to data set A and the dashed line is for the *R*-matrix fit to data set B. For comparison to the *R*-matrix fits the data were scaled by 1.04.

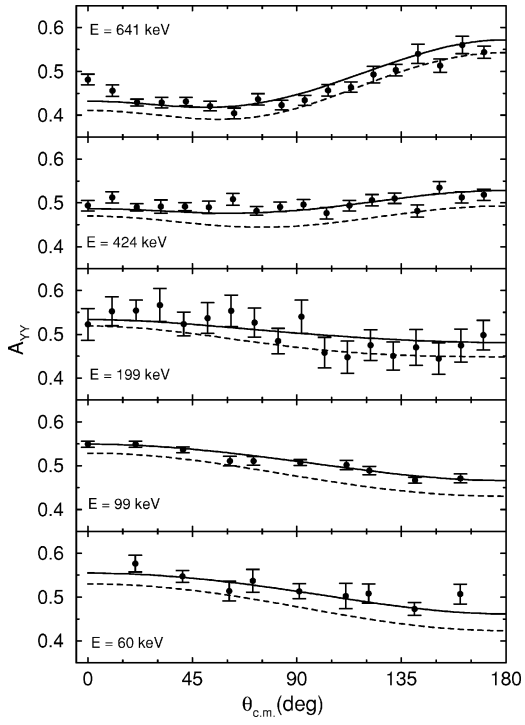


FIG. 7. Angular distributions of $A_{yy}$ for the $^3$He$(d,p)^4$He reaction. The solid line shows an *R*-matrix fit to data set A and the dashed line is for the *R*-matrix fit to data set B. For comparison to the *R*-matrix fits the data were scaled by 1.03.

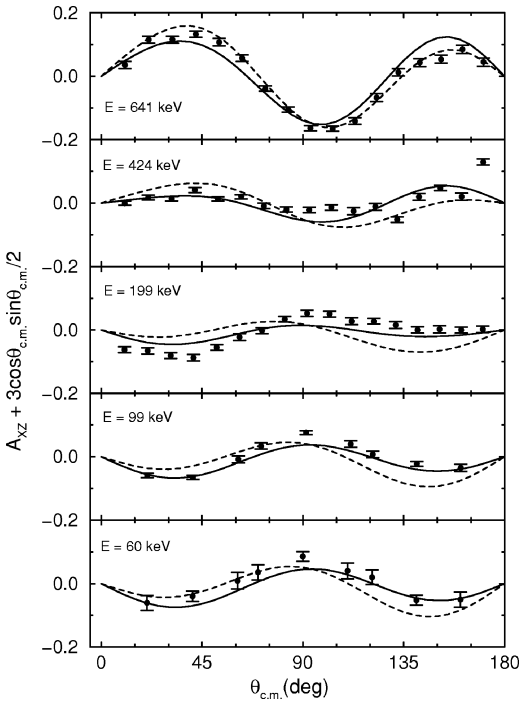


FIG. 9. Angular distributions of $A_{xz}$ (modified as described in the text) for the $^3$He$(d,p)^4$He reaction. The solid line shows an *R*-matrix fit to data set A and the dashed line is for the *R*-matrix fit to data set B. For comparison to the *R*-matrix fits the data were scaled by 1.04.

TABLE II. The data used with the present *R*-matrix analysis, data set A.

| Reaction | Energy range (MeV) | No. observables | No. data points | References |
|---|---|---|---|---|
| $^3$He$(d,d)^3$He | $E_d=0-1$ | 1 | 128 | [48,49] |
| $^3$He$(d,p)^4$He | $E_d=0-1$ | 10 | 892 | [2,3,8,10,12,14,50,51] |
| $^3$He$(d,p)^4$He | $E_d=0-1$ | 5 | 349 | present work |
| $^4$He$(p,p)^4$He | $E_p=0-24$ | 3 | 562 | [52–55] |
| Total | | 14 | 1931 | |

than the other data sets. Also the present data have been measured to a greater precision than the previous measurements, especially $A_y$. These VAP data reveal a rather constant maximum value over the entire energy range of this study.

## IV. ANALYSIS

The current data have been included in the data set used by the LANL multichannel *R*-matrix parametrization of the $A=5$ system. A review of the *R*-matrix formalism is discussed in Ref. [29] and the specific LANL *R*-matrix approach is described in Ref. [30]. A brief summary is given here. The elements of the *R* matrix are given by

$$R_{c'c}=\sum_{\lambda}\frac{\gamma_{\lambda c'}\gamma_{\lambda c}}{E_\lambda-E}. \tag{9}$$

The data are fit by varying the *R*-matrix parameters: the reduced-width amplitudes $\gamma_{\lambda c}$ and energies $E_\lambda$ for the reaction channel $c$ and energy level $\lambda$, until the best fit is obtained to the data set as determined by a minimization of the $\chi^2$. The data set contains total and differential cross sections, VAP and TAPs, and spin correlation coefficients and is listed in Table II. The present VAP and TAPs below 300 keV were the first data of this type to be included in the LANL analysis of $^5$Li.

Once the best-fit parameters are found, the parameterization can then be used to predict unmeasured observables and to obtain the level structure of $^5$Li. The levels were obtained from the ''extended'' *R*-matrix method [31,32] that uses the complex poles and residues of the *S* matrix. This prescription results in resonance parameters that are free from the geometric parameters of *R*-matrix theory, such as the channel radii and boundary conditions.

The data set used in the present *R*-matrix parametrization, shown in Table II, will be referred to as data set A. Also included in the figures is a previously determined *R*-matrix parametrization based on a data set described in Ref. [33] which will be referred to as data set B. It should be noted that these two data sets contain different data and span somewhat different excitation energies in $^5$Li. Data set B contains data up to 28 MeV of excitation in $^5$Li, but includes limited data for the $^3$He$(d,p)^4$He reaction below 1 MeV. Data set A was constructed from data set B by truncating it at an excitation energy of $\sim$18 MeV but including the present data along with other data for the $^3$He$(d,p)^4$He reaction. Data set A was truncated in order to simplify the fitting of the lower-energy data which corresponds to the energy range of interest. In the *R*-matrix analysis of data set A the data points were allowed to be scaled within their systematic errors and the data shown in the figures were renormalized by these values. As expected (see Figs. 4–9), the *R*-matrix fits to data set A describe these low-energy data better than fits to data set B. The highest partial waves allowed in the entrance channel is $L=2$, while for the exit channel up to $L=4$ was allowed. The best-fit *R*-matrix parametrization achieved a minimum $\chi^2$ per degree of freedom $\chi^2_\nu$ less than 1.8.

## V. DISCUSSION

### A. States of $^5$Li

The level structures obtained from the *R*-matrix analysis using the two data sets are listed in Table III. Compared to the data set B parametrization, the $\frac{3}{2}^+$ level has shifted to a slightly lower energy, and corresponds to a calculated peak cross section for the $^3$He$(d,p)^4$He reaction located at $E_d=413$ keV, lower than the earlier value of $E_d=430$ keV [34]. The first two levels in $^5$Li are similar for solutions A and B, as expected since these levels are determined mainly by the lower-energy $p+^4$He scattering data that are the same in both data sets. The two solutions exhibit larger variations in the position and width of the first excited state ($\frac{1}{2}^-$) because it is so broad.

One quantitative difference between the two level schemes is the presence of a $\frac{1}{2}^+$ level located below 17 MeV excitation energy. This is a weak resonance (pole strength $\approx$0.14), and its position may be quite uncertain. For a $\frac{1}{2}^+$ *S*-wave resonance interfering with a $\frac{3}{2}^+$ *S*-wave resonance, the cross section would be isotropic and the analyzing powers would only differ by a scale factor from that for a pure $\frac{3}{2}^+$ *S*-wave resonance. Since the level scheme derived from

TABLE III. The scheme of levels in $^5$Li below $E_x=17$ MeV. The present scheme is obtained from an *R*-matrix analysis using data set A and the previous scheme is from an *R*-matrix analysis using data set B [33] .

| Previous scheme | | | Present scheme | | |
|---|---|---|---|---|---|
| $E_x$ (MeV) | $J^\pi$ | $\Gamma_{\text{c.m.}}$ (MeV) | $E_x$ (MeV) | $J^\pi$ | $\Gamma_{\text{c.m.}}$ (MeV) |
| g.s | $\frac{3}{2}^-$ | 1.23 | g.s | $\frac{3}{2}^-$ | 1.25 |
| 1.49 | $\frac{1}{2}^-$ | 6.60 | 1.28 | $\frac{1}{2}^-$ | 6.29 |
| 16.87 | $\frac{3}{2}^+$ | 0.27 | 16.86 | $\frac{3}{2}^+$ | 0.25 |
| 20.53 | $\frac{1}{2}^+$ | 5.00 | 16.88 [a] | $\frac{1}{2}^+$ | 2.26 |
| 19.28 | $\frac{3}{2}^-$ | 0.96 | 17.65[a,b] | $\frac{3}{2}^-$ | 2.57 |
| 19.45 | $\frac{7}{2}^+$ | 3.28 | | | |

[a]Weak resonance.

[b]Above the range of the analysis.

data set B contained very little analyzing power data below 1 MeV, it would not be as sensitive to a $\frac{1}{2}^+$ level as the present scheme derived from data set A. However, both solutions indicate that a broad $\frac{1}{2}^+$ level exists somewhere in the 16-21 MeV range of excitation energy, which may correspond to the possible $\frac{1}{2}^+$ resonant state in $^5$Li at $E_d \approx 1-3$ MeV that was discussed in Ref. [38].

The new analysis also predicts another $\frac{1}{2}^+$ state about 800 keV below the $d+^3$He threshold. This level is virtual in the closed $d+^3$He channel (i.e., on the second sheet), so it would not show up as a resonance in the $p+^4$He scattering data. We mention this pole, despite the weak experimental evidence for its existence, because it is suggestive of the subthreshold $\frac{1}{2}^+$ state that has been seen in some shell-model calculations [35–37] for the $A=5$ system.

We also list in Table III a weak $J^\pi = \frac{3}{2}^-$ level, although it is above the range of the analysis. There is also evidence for a $\frac{7}{2}^+$ state somewhat higher in excitation energy. These are in qualitative agreement with the results for data set B. The $3/2^-$ state, which is primarily in the $^2P(d)$ channel, is the first negative-parity resonance that occurs above the $d+^3$He threshold. The interference of this level with the low-lying positive-parity states is primarily responsible for the asymmetry about $90^o$ in the $^3$He$(d,p)^4$He scattering observables, such as that seen for $A_{yy}$ in Fig. 7.

### B. Electron screening effects

The enhancement of the experimental cross section $\sigma_{\rm exp}(E)$ over the bare-nuclear cross section $\sigma_{\rm BN}(E)$ is represented by the enhancement factor $f(E)$ defined as

$$f(E)=\frac{\sigma_{\rm exp}(E)}{\sigma_{\rm BN}(E)}. \tag{10}$$

To determine the screening enhancement from experimental cross section data, $\sigma_{\rm BN}$ needs to be known near zero energy. It is convenient to represent $\sigma_{\rm BN}$ in terms of the astrophysical $S$-factor defined by

$$\sigma_{\rm BN}(E)=\frac{S(E)}{E}\exp[-2\pi\eta(E)], \tag{11}$$

where $2\pi\eta(E)=31.29Z_1Z_2\sqrt{\mu/E}$, $Z_1$ and $Z_2$ are the atomic numbers of the interacting particles in the entrance channel, $\mu$ is the reduced mass in units of amu, and $E$ is the center-of-mass energy in keV. The $S$ factor is typically slowly varying at low energies in contrast to the cross section which drops exponentially with decreasing energy because of the Coulomb barrier. A screening potential $U_e$ can also be defined [39,40] such that $\sigma_{\rm exp}(E)=\sigma_{\rm BN}(E+U_e)$. The screening enhancement is then given approximately by [40,41]

$$f(E)=\exp[\pi\eta(E)U_e/E]. \tag{12}$$

It should be noted that $U_e$ is expected theoretically to be somewhat dependent on the bombarding energy [40]; however, all experimental analyses including the present one assume constant $U_e$. The value of $f(E)$ approaches unity at high energies in which case the laboratory measurements can be assumed to represent $\sigma_{\rm BN}(E)$. For lower energies $\sigma_{\rm BN}(E)$ can be determined by extrapolation of the higher-energy data to the energy range of interest.

From the present $R$-matrix parametrization, the cross section can be calculated down to near zero energy and a screening factor can be calculated. In all of the previous electron screening determinations, $\sigma_{\rm BN}$ was determined by extrapolating fits to only higher-energy $^3$He$(d,p)^4$He cross section data. The extrapolation by Chulick *et al.* [42] which is used in the most recent screening determinations [43] was made by fitting all of the cross section data existing at the the time of publication of Ref. [42]. This data set includes measurements that in some cases show substantial disagreement with each other.

There have been several theoretical calculations of the screening potential for the $^3$He$(d,p)^4$He reaction [44,40,45]. A simple model to calculate this potential assumes that the classical turning radius of a projectile for a bare nucleus is larger than the atomic radius. Then $U_e \approx Z_1Z_2e^2/R_a$ where $R_a$ is the radius of the inner electrons of the target atom. In this case $U_e \approx 110$ eV depending on $R_a$ [15]. Currently, the theoretical calculation that predicts the largest $U_e$ value is from the adiabatic limit [44]. In this model $U_e$ is equal to the difference in electron binding energy between the target and the combined projectile-target system and is calculated to be 119 eV for the $^3$He$(d,p)^4$He reaction. It should be noted that all of the calculations of which we are aware assume that the incident deuteron is fully ionized—an assumption which may not be valid as the beam passes through the target material.

The screening potential $U_e$ was determined from the $R$-matrix parametrization and the experimental cross sections using the following procedure. The $S$-factor was calculated from Eq. (11) and the $R$-matrix parametrization and then parametrized from $0 \leqslant E \leqslant 60$ keV by the expression

$$S(E)=6.70+2.43\times10^{-2}E+2.06\times10^{-4}E^2, \tag{13}$$

where $E$ is the center-of-mass energy in keV and $S(E)$ is in units of MeV b. The experimental $S(E)$ data reported in Ref. [43][1] were used and the data were allowed to scale within a reasonable range, explained below, because the $S$-factor calculated from the $R$-matrix parametrization is noticeably larger than the data. The screening potential was determined by fitting $U_e$ and an absolute scale factor for the data, using $\sigma_{\rm exp}(E)=\sigma_{\rm BN}(E+U_e)$ in conjunction with Eqs. (11) and (13). The fit is shown in Fig. 10 and yielded $U_e=177 \pm 29$ eV with a scale factor of 1.165 and a $\chi^2_\nu$ of 4.5. The error is defined as the difference in the screening potential when the $\chi^2$ increased by one from the best fit value.

One may question if scaling the experimental data is justified. The normalization by a factor of 1.165 needed with the $R$-matrix calculation is outside the quoted 7.1% uncer-

[1]These data were originally reported in Ref. [15] and corrected in Ref. [43] to take into account new stopping-power measurements [46]. The data used in the present calculation have only statistical errors included.

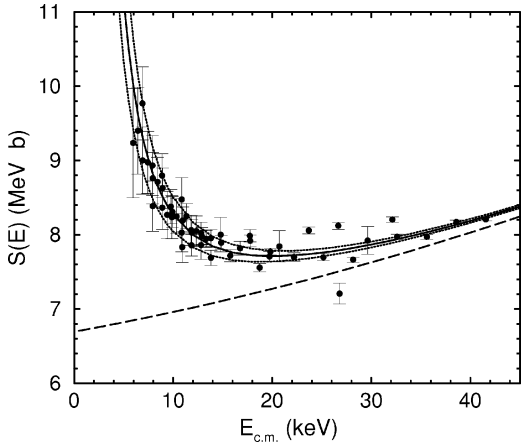


FIG. 10. Electron screening calculations using *R*-matrix calculations for the bare nuclear cross section (dashed line) and the data from Ref. [43](solid circles). The data were scaled by a factor of 1.165 resulting in $U_e = 177 \pm 29$ eV with a $\chi^2_\nu$ of 4.5. The solid line is the calculated enhancement for a screening potential of $U_e = 177$ eV, while the dotted lines show the error.

tainty in Ref. [15] but is not unreasonable considering that there is also some uncertainty in the normalization of the *R*-matrix parametrization. Furthermore the data of Ref. [43] show a very large systematic scatter for $E > 20$ keV which complicates the determination of the normalization (see Fig. 10). In addition, data at very low energies are notoriously difficult to obtain accurately because of the extremely low cross sections involved. There are also difficulties in determining the reaction energy because of energy losses in the target.

The present determination of the screening potential is much larger than 119 eV, the screening value calculated from the adiabatic limit. Measurements of larger screening potential values than theoretical models can predict have been a persistent puzzle and are seen for many other reactions [47]. The present determination is also in disagreement with the most recently determined value of $130 \pm 8$ eV [43]. In Ref. [43], an extrapolation of the cross section from Ref. [42] was used for the bare nuclear cross section and the experimental data were not allowed to scale. A scale factor should have been allowed for in their determination because the experimental data were normalized to one data set [14], while the bare nuclear cross section is derived from many different data sets that have different absolute normalizations. The need for a scale factor is seen by the fact that the majority of the experimental data points above $E = 20$ keV fall below the calculated *S* factor [43]. We have performed an additional screening determination, similar to that of Ref. [43], using instead of the *R* matrix $\sigma_{\mathrm{BN}}$ the extrapolation given in Ref. [42] for $\sigma_{\mathrm{BN}}$ and allowing for the experimental data to be scaled. This procedure resulted in $U_e = 170 \pm 28$ eV with the data scaled by only 1.03 and a $\chi^2_\nu$ of 4.7. It is important to note that a small change of only 3% in the absolute scale of the data changes the extracted $U_e$ from 130 to 170 eV. This result is in excellent agreement with the present determination of $177 \pm 29$ eV using our *R*-matrix parametrization for $\sigma_{\mathrm{BN}}$. In summary, we derive a significantly larger screening potential than reported in Ref. [43], but this difference arises mainly from allowing the normalization of the data to float relative to $\sigma_{\mathrm{BN}}$, rather than the assumed energy dependence of $\sigma_{\mathrm{BN}}$.

## VI. SUMMARY

Angular distributions of cross sections and complete sets of analyzing powers ($A_y$, $A_{yy}$, $A_{zz}$, and $A_{xz}$) for the $^3$He$(d,p)^4$He reaction have been measured at mean laboratory reaction energies of 60, 99, 199, 424, and 641 keV. Measurements of the energy dependence of the cross section have also been performed from 245 to 685 keV and the value of the total cross section has been measured to be $777 \pm 33$ mb at $E_d = 426$ keV. The present cross section and analyzing power data are more precise but generally consistent with previously obtained data, where they exist.

The present data have been included in a global *R*-matrix analysis of the $^5$Li system, from which a new level structure of $^5$Li has been determined. It is found that the $\frac{3}{2}^+$ level in $^5$Li is located at a lower energy than reported in Ref. [34]. The corresponding peak cross section for the $^3$He$(d,p)^4$He reaction occurs at $E_d = 413$ keV. Also, evidence for a subthreshold $\frac{1}{2}^+$ level is found. From the *R*-matrix analysis, a calculation of the astrophysical *S* factor down to zero energy was made and is given by Eq. (13). This *S*-factor determination was used in an electron screening determination resulting in a screening potential of $177 \pm 29$ eV. This value is larger than existing theoretical models predict, a persistent trend that is seen with several other reactions. We emphasize that the $^3$He$(d,p)^4$He reaction is the best known experimental case for studying electron screening. Additional improved low-energy cross section data are required to confirm the disagreement with theoretical predictions.

## ACKNOWLEDGMENTS

The authors would like to thank Z. Ayer, B. J. Crowe, S. E. Hale, L. Ma, D. C. Powell, and M. H. Wood for their assistance in the data collection process. One of us (W.H.G.) thanks group T-2 at Los Alamos for their support during the *R*-matrix calculations. This work was supported in part by the U. S. Department of Energy, Office of High Energy and Nuclear Physics, at TUNL under Grant Nos. DE-FG05-88ER40442 and DE-FG02-97ER41041, and at LANL under Grant No. KB04.

[1] H. E. Conzett, in *Few Body Problems in Physics: Proceedings of the 10th International IUPAP Conference on Few Body Problems in Physics, Vol. II*, Karlsruhe, Germany, 1983, edited by B. Zeitnitz (North-Holland, Amsterdam, 1984), p. 539.

[2] Ch. Leemann, H. Bürgisser, P. Huber, U. Rohrer, H. Paetz gen. Schieck, and F. Seiler, Phys. Acta **44**, 141 (1971); An apparent sign error in Eq. (4) of this article for odd values of $m+M$ has led to confusion about the sign of the vector analyzing power

found by this measurement.
[3] R. Garrett and W. W. Lindstrom, Nucl. Phys. **224**, 186 (1974).
[4] M. P. Rekalo and E. Tomasi-Gustafsson, Phys. Rev. C **57**, 2870 (1998).
[5] M. S. Smith, L. H. Kawano, and R. A. Malaney, Astrophys. J., Suppl. Ser. **85**, 219 (1993).
[6] S. Burles and D. Tytler, Astrophys. J. **499**, 699 (1998).
[7] T. W. Bonner, J. P. Conner, and A. B. Lillie, Phys. Rev. **88**, 473 (1952).
[8] J. L. Yarnell, R. H. Lovberg, and W. R. Stratton, Phys. Rev. **90**, 292 (1953).
[9] G. Freier and H. Holmgren, Phys. Rev. **93**, 825 (1954).
[10] W. E. Kunz, Phys. Rev. **97**, 456 (1955).
[11] L. Zichang, Y. Jingang, and D. Xunliang, Chin. J. Sci. Technique Atomic Energy **3**, 229 (1977).
[12] W. Möller and F. Besenbacher, Nucl. Instrum. Methods Phys. Res. **168**, 111 (1980).
[13] J. A. Davies and P. R. Norton, Nucl. Instrum. Methods Phys. Res. **168**, 611 (1980).
[14] A. Krauss, H. W. Becker, H. P. Trautvetter, C. Rolfs, and K. Brand, Nucl. Instrum. Methods Phys. Res. A **465**, 150 (1987).
[15] S. Engstler, G. Raimann, K. Neldner, C. Rolfs, U. Schröder, and K. Langanke, Phys. Lett. B **202**, 179 (1988).
[16] W. Geist, Z. Ayer, A. C. Hird, H. J. Karwowski, and E. J. Ludwig, Nucl. Instrum. Methods Phys. Res. A **365**, 36 (1995).
[17] L. J. Dries, H. W. Clark, R. Detomo, Jr., J. L. Regner, and T. R. Donoghue, Phys. Rev. C **21**, 475 (1980).
[18] T. B. Clegg, H. J. Karwowski, S. K. Lemieux, R. W. Sayer, E. R. Crosson, W. M. Hooke, C. R. Howell, H. W. Lewis, A. W. Lovette, H. J. Pfutzner, K. A. Sweeton, and W. S. Wilburn, Nucl. Instrum. Methods Phys. Res. A **357**, 200 (1995).
[19] T. C. Black, B. E. Hendrix, E. R. Crosson, K. A. Fletcher, H. J. Karwowski, and E. J. Ludwig, Nucl. Instrum. Methods Phys. Res. A **333**, 239 (1993).
[20] E. J. Ludwig, T. C. Black, C. R. Brune, W. H. Geist, and H. J. Karwowski, Nucl. Instrum. Methods Phys. Res. A **388**, 37 (1997).
[21] M. Uhrmacher, K. Pampus, F. J. Bergmeister, D. Purschke, and K. P. Lieb, Nucl. Instrum. Methods Phys. Res. B **9**, 234 (1985).
[22] W. H. Geist, Ph. D. thesis, University of North Carolina at Chapel Hill, 1998, Available from University Microfilms, Ann Arbor, Michigan.
[23] W. H. Geist, Z. Ayer, A. C. Hird, E. J. Ludwig, M. Wood, and K. A. Fletcher, Nucl. Instrum. Methods Phys. Res. B **111**, 176 (1996).
[24] J. P. Biersack and L. G. Haggmark, Nucl. Instrum. Methods Phys. Res. **174**, 257 (1980).
[25] T. C. Black, Ph.D. thesis, University of North Carolina at Chapel Hill, 1995, Available from University Microfilms, Ann Arbor, Michigan.
[26] D. G. Sargood, Phys. Rep. **93**, 61 (1982).
[27] R. E. Brown and N. Jarmie, Phys. Rev. C **41**, 1391 (1990).
[28] M. Bittcher, W. Grüebler, V. König, P. A. Schmelzbach, B. Vuaridel, and J. Ulbricht, Few-Body Syst. **9**, 165 (1990).
[29] A. M. Lane and R. G. Thomas, Rev. Mod. Phys. **30**, 257 (1958).
[30] G. M. Hale and D. C. Dodder, in *Proceedings of the International Conference on Nuclear Cross Sections for Technology*, Knoxville, 1979, edited by J. L. Fowler, C. H. Johnson, and C. D. Bowman, Natl. Bur. Stand. (U.S.) Spec. Publ. No. 594 (U.S. GPO, Washington, D.C., 1980), p. 650.
[31] G. M. Hale, R. E. Brown, and N. Jarmie, Phys. Rev. Lett. **59**, 763 (1987).
[32] A. Csótó and G. M. Hale, Phys. Rev. C **55**, 536 (1997).
[33] D. R. Tilley, C. M. Cheves, and G. M. Hale (unpublished).
[34] F. Ajzenberg-Selove, Nucl. Phys. **A490**, 1 (1988).
[35] A. G. M. van Hees and P. W. M. Glaudemans, Z. Phys. A **314**, 323 (1983).
[36] A. G. M. van Hees and P. W. M. Glaudemans, Z. Phys. A **315**, 223 (1984).
[37] F. C. Barker and C. L. Woods, Aust. J. Phys. **38**, 563 (1985).
[38] L. C. McIntyre and W. Haeberli, Nucl. Phys. **A91**, 369 (1967).
[39] H. J. Assenbaum, K. Langanke, and C. Rolfs, Z. Phys. A **327**, 461 (1987).
[40] T. D. Shoppa, S. E. Koonin, K. Langanke, and R. Seki, Phys. Rev. C **48**, 837 (1993).
[41] S. Engstler, G. Raimann, C. Angulo, U. Greife, C. Rolfs, U. Schröder, E. Somorjai, B. Kirch, and K. Langanke, Z. Phys. A **342**, 471 (1992).
[42] G. S. Chulick, Y. E. Kim, R. A. Rice, and M. Rabinowitz, Nucl. Phys. **A551**, 255 (1993).
[43] K. Langanke, T. D. Shoppa, C. A. Barnes, and C. Rolfs, Phys. Lett. B **369**, 211 (1996).
[44] L. Bracci, G. Fiornetini, V. S. Melezhik, G. Mezzorani, and P. Quarati, Nucl. Phys. **A513**, 316 (1990).
[45] K. Langanke and D. Lukas, Ann. Phys. (N.Y.) **1**, 332 (1992).
[46] R. Golser and D. Semrad, Phys. Rev. Lett. **66**, 1831 (1991).
[47] C. Rolfs and E. Somorjai, Nucl. Instrum. Methods Phys. Res. B **99**, 297 (1995).
[48] L. Kraus, Ph.D. thesis, Université Louis Pasteur, Strasbourg, 1971, Thése No. 681.
[49] R. J. S. Brown, K. F. Famularo, H. D. Holmgren, D. Rankin, and T. F. Stratton, Phys. Rev. **96**, 80 (1954).
[50] B. Forssmann, G. Graf, H. Schober, and H. P. Jochim, *Proceedings of the Third International Symposium on Polarization Phenomena in Nuclear Reactions*, Madison, WI, 1970, edited by H. H. Barschall and W. Haeberli (University of Wisconsin Press, Madison, 1970), p. 537.
[51] G. G. Ohlsen, J. L. McKibben, and G. P. Lawrence, *Proceedings of the Third International Symposium on Polarization Phenomena in Nuclear Reactions*, Madison, WI, 1970, edited by H. H. Barschall and W. Haeberli (University of Wisconsin Press, Madison, 1970), p. 503.
[52] A. C. L. Barnard, C. M. Jones, and J. L. Weil, Nucl. Phys. **50**, 604 (1964).
[53] D. Garreta, J. Sure, and A. Tarrats, Nucl. Phys. **A132**, 204 (1969).
[54] G. R. Plattner, A. D. Bacher, and H. E. Conzett, Phys. Rev. C **5**, 1158 (1972).
[55] L. Brown and W. Trächslin, Nucl. Phys. **A90**, 334 (1967).